

Flash melting of tantalum in a diamond cell to 85 GPaAmol Karandikar^{1,2,*} and Reinhard Boehler¹¹*Geophysical Laboratory, Carnegie Institution of Washington, 5251 Broad Branch Road NW, Washington DC 20015, USA*²*Geowissenschaften, Goethe-Universität, Altenhöferallee 1, D-60438 Frankfurt a.M., Germany*

(Received 15 April 2015; revised manuscript received 11 January 2016; published 9 February 2016)

We demonstrate a new level of precision in measuring melting temperatures at high pressure using laser flash heating in a diamond cell followed by an analysis using scanning electron microscopy and focused ion beam milling. The new measurements on tantalum put unprecedented constraints on its highly debated melting slope, calling for a reevaluation of theoretical, shock compression, and diamond cell approaches to determine melting at high pressure. X-ray analysis of the recovered samples confirmed the absence of chemical reactions, which likely played a significant role in previous experiments.

DOI: [10.1103/PhysRevB.93.054107](https://doi.org/10.1103/PhysRevB.93.054107)**I. INTRODUCTION**

The unusually large discrepancies in the melting temperatures of tantalum (Ta) and some other transition metals at high pressures have challenged our understanding of not only the high temperature properties of metals relevant to bonding and structure but also of our experimental and theoretical approaches to determine melting temperatures at high pressure [1–17]. Particularly for Ta, the differences among results from static measurements in the diamond cell, and shock experiments are too large to be explained by experimental errors, and a large spread in melting slopes from various theoretical results underlines the difficulties in predicting melting.

Most measurements on Ta melting in the laser-heated diamond anvil cell (LHDAC) using optical and textural observations [1,18] and synchrotron x-ray diffraction (XRD) [19] have produced flat melting curves ($dT/dP \rightarrow 0$) with one exception [20]. Both shock data and theory have predicted steep but strongly varying melting slopes. Figure 1 shows all results from static and shock experiments [21–23] and from theory [3,4,6,7,9,11,13,14,16,24].

There have been a number of suggestions to reinterpret the observation of low melting temperatures as being due to phase transitions from body-centered cubic (bcc) to other energetically favorable but debated structures [10,15,16,25–29]. However, *in situ* XRD measurements in the DAC to 174 GPa at 300 K [31] and to 135 GPa at 5800 K [20] and calculations to 1 TPa at 0 K [30] have not reported any phase other than bcc.

The only methods for measuring melting at very high pressure-temperature (P-T) conditions are shock measurements and the LHDAC technique. Problems associated with these techniques are the short time scale and chemical contamination of Ta, respectively. Previous LHDAC studies [1,18] that attributed melting to optical observations of textural changes on the sample surface lacked chemical analysis, and from our present observations, chemical contaminations of Ta during prolonged heating were highly likely in these studies. The *in situ* XRD measurements in the LHDAC [20] that reported the only experimental steep melting curve relied on the appear-

ance of a diffuse scattering ring and/or diffraction spots arising from fast recrystallization [20,32]. The main difficulty in such experiments is to confine and stabilize the melted portion of the sample long enough to document melting. However, heating durations of even a few seconds near the melting temperature causes sample instabilities such as ‘hole burning’ and dispersion of melt into the surrounding pressure medium. These instabilities inevitably cause misalignment of the sample hotspot with the x-ray beam and the spectrometer to measure temperature, leading to large experimental uncertainties [20]. Moreover, the same XRD work reports chemical reactions to be unavoidable, with the x-ray acquisitions lasting for a few tens of seconds during continuous wave (CW) heating.

A recent technique of flash heating in the LHDAC [33] circumvented these difficulties by reducing heating durations to milliseconds, yet measuring temperatures accurately. Sample recovery and subsequent analysis using scanning electron microscopy (SEM) with energy dispersive x-ray (EDX) spectroscopy unambiguously identified melting in the absence of chemical reactions and yielded accurate melting temperatures of rhenium (Re) and molybdenum at 1 atm and up to 50 GPa. In the present flash-heating experiments on Ta, we improved the measurement setup and extended the analysis using focused ion beam milling (FIBM), showing unambiguously the onset of melting and the extent of melt in depth. Here, we report precise melting measurements from 1 atm to 85 GPa without any sign of chemical alteration. Combining flash heating with chemical, textural, and depth-profile analysis of the recovered samples drastically reduced the experimental uncertainties compared to previous measurements.

II. EXPERIMENTAL

A Ta disc (diameter 25–45 μm , 5–8 μm thick), laser cut from a polished foil (Alfa Aesar 99.95% purity), resting on a plate of single crystal sapphire (3–5 μm thick, 40–60 μm wide) was placed on one of the diamond anvils. Re gaskets, preindented to 35 μm , were used in a plate-DAC [34] with culet sizes 250–300 μm . The cells were loaded with 99.999% purity argon as a pressure transmitting medium. Ruby grains (2–3 μm size) placed close to the sample served as pressure markers. Above 35 GPa, the Raman signal of diamond was additionally used for pressure measurements [35]. Pressures measured before and after heating experiment did not differ

* Author for correspondence: akaran@carnegiescience.edu

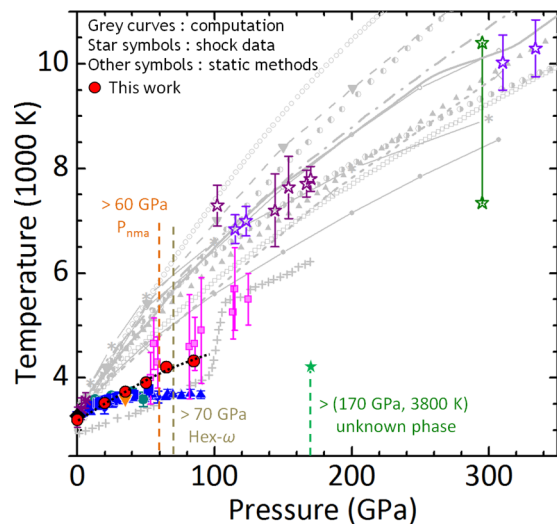


FIG. 1. Ta melting from theory, and static and shock data to date. THEORY: Generalized Lindemann: solid gray line [3]. Dislocation mediated melting: dashed gray line with down triangles [7], open gray square [14]. Vacancy formation enthalpy calculation: gray line with asterisks [6]. Quantum atomistic: dashed-dotted gray line [4]. First principles density functional theory - generalized gradient approximation (DFT-GGA)/projector augmented-wave (PAW): dashed gray line with Xs [11]. Coexistence phase molecular dynamics (MD) simulations: solid gray line with filled circles, extended Finnis-Sinclair (EFS) potential; solid gray line with open circles, force matching (FM) potential; open circles, long-range empirical potential (LREP) [13]. *Ab initio* MD: right-filled circle, bcc; left-filled circle, hex- ω [16]. DFT - model generalized pseudopotential theory (MGPT) MD: filled up triangles [24]. STATIC DATA: 1 atm, filled black diamonds [37,38]. Drickamer piston cylinder: purple starbursts [40]. Speckle method: blue filled up triangles [1]; bead formation: blue filled circles [1]; teal filled circles [18]. XRD: blue filled squares [19]; pink filled squares [20]. Laser power anomaly: yellow filled down triangles [9]. SHOCK DATA: T calculated with heat capacity models: green open stars [21]; T pyrometric: violet open stars [22]; simultaneous Hugoniot-T measurement: purple open stars [23]. Vertical dashed lines indicate predicted phase transition pressures for hex- ω [16], P_{nma} [26,27], and an unidentified speculated phase [10]. Phase boundary between bcc and shear induced plastic flow: gray plus signs [15]. Flash-melting data measured in this paper: filled red circles. The total uncertainty for each flash-melting temperature is smaller than the symbol size (≈ 200 K). Black dotted line is a guide to the eye.

by more than 2 GPa. We assume that the thermal pressure is low due to the small volume ratio of the heated sample portion to surrounding argon with low shear strength [36].

Figure 2 schematically shows the optical setup for flash heating in the diamond cell. An ytterbium fiber laser ($\lambda = 1070$ nm, TEM₀₀ mode, CW, IPG Photonics), was triggered and modulated by a pulse generator (TENMA TGP110) producing a rectangular pulse of 20 ms duration. The laser emission and the corresponding thermal response of the sample were simultaneously measured by a photo diode (PD) and a photomultiplier tube (PMT), respectively and monitored with an oscilloscope. (Fig. 2, inset iv). This heating duration, called flash, is long enough to measure temperatures reliably

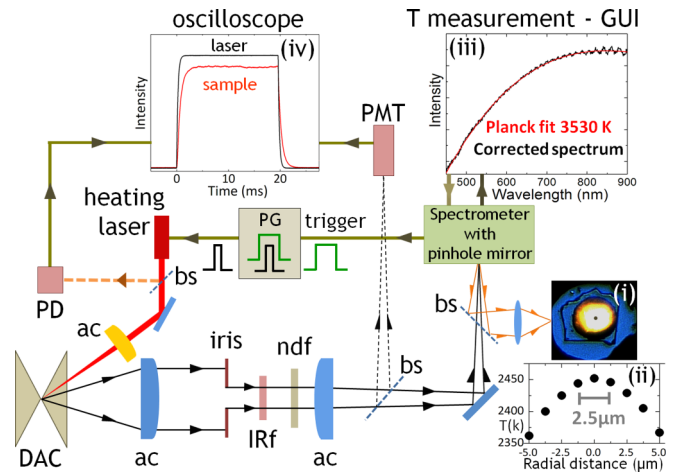


FIG. 2. Schematics of the experimental setup for single-flash heating in the LHDAC. A graphic user interface (GUI) command opens the shutter of the spectrometer to measure temperature and simultaneously triggers a pulse generator (PG) that controls the heating laser to produce a 20 ms rectangular pulse. A pair of achromats (ac) collects the thermal radiation from the central area (diameter $\approx 3\mu\text{m}$) of the hot spot (inset i), which is aligned to the pinhole at the spectrometer entrance. Temperature profiles measured across the hot spot (inset ii) show gradients of <10 K over the central area. An infrared filter (IRf) and neutral density filters (ndf) filter out laser radiation and avoid oversaturation of the spectrometer, respectively. An iris minimizes chromatic aberration [41], allowing accurate temperature measurements in the wavelength range 450–900 nm (inset iii) using a CCD. A PD and PMT record the 20 ms laser pulse and the corresponding thermal response from the sample, respectively (inset iv). The blue dashed-lined elements (bs) are beam splitters.

and short enough to avoid chemical reactions or sample instability. The flash heating and the temperature measurement were synchronized such that the thermal response of the sample during 20 ms is fully recorded by the spectrometer. The sample reached a constant temperature in less than 2 ms. The rise and fall times of the thermal response, monitored by a PMT, contribute $<1\%$ to the total spectral intensity. Further details of the optical setup and temperature measurement can be found elsewhere [33].

The procedure for the flash-melting measurements was as follows: Microscope images of the sample (Ta disc) were recorded before loading in the diamond cell and after pressurizing to the desired pressure. For an optical alignment, the laser power was adjusted to create a hotspot on the sample at temperatures below the ambient melting temperature of Ta to avoid any modification of the sample. Further, the laser focus was adjusted (Fig. 2, i) to obtain a temperature gradient of <10 K over the central area (diameter $3\mu\text{m}$) of the hot spot (Fig. 2, ii) from which the temperatures were measured with a calibrated charge-coupled device (CCD) spectrometer. The sample was then heated with a higher laser power in a single flash event of 20 ms while recording the temperature (Fig. 2, iii). Microscope images of the sample were recorded after this event and after sample recovery. The recovered sample was then analyzed using SEM (JEOL JSM-6500F and Zeiss Auriga 40) for surface texture and FIBM (Zeiss Auriga 40) for depth profiling, measuring the extent of melt. Chemical analysis of

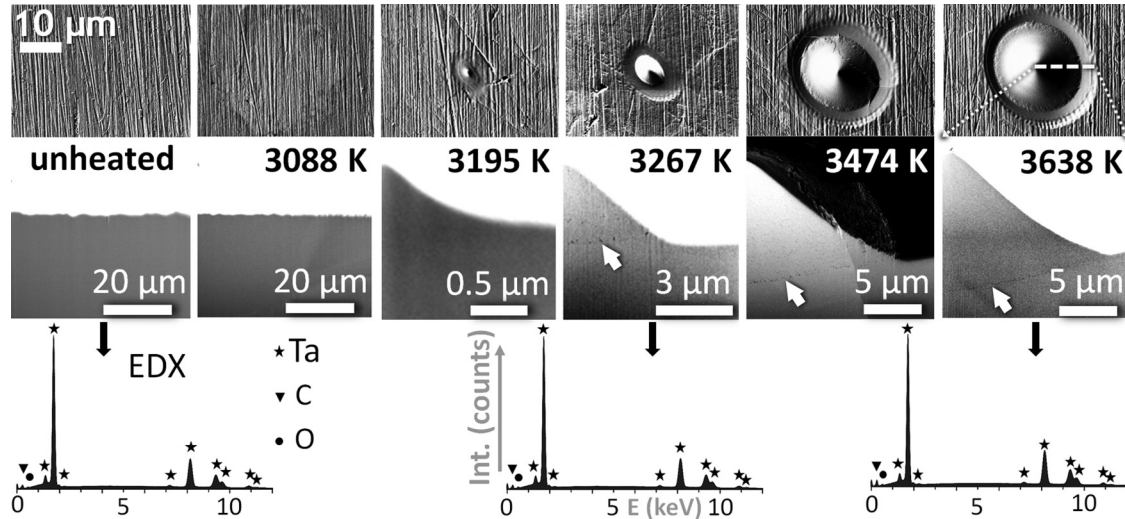


FIG. 3. Ta foil, flash heated in argon flow at 1 atm, probed by SEM, FIBM, and EDX. Row 1: SEM images of different flash-heated areas at increasing temperatures. Scale shown is for the entire row. At 3195 K, the first textural modification is observed. Row 2: Respective FIB cross sections cut across the features shown in row 1. For simplicity, only half of the cross sections are shown. The modification at 3195 K is too small to identify any features in depth. At 3267 K, close to the known melting point of Ta (3270 K), a crater formed showing substantial restructuring of material with about a $3\ \mu\text{m}$ deep sharp boundary between the unmolten solid and quenched liquid. Spots heated below 3195 K showed no textural change in their FIB profiles, whereas those above 3267 K show restructuring of the sample with a sharp boundary growing both laterally and in depth, with increasing temperature. Row 3: EDX spectra from unheated and heated portions indicating absence of any chemical reaction at and above melting.

Ta was done using EDX (JEOL JSM-6500F) on the heated portions on the surface and in the interior exposed by FIB cuts. This procedure was repeated with new samples at a given pressure until a temperature range was covered spanning about 400 K below and above a temperature at which a first smooth textured modification appeared in the heated area indicating melting as described in detail in Results. Flash-heating runs were carried out at 20, 22, 32, 35, 50, 65, and 85 GPa (Fig. 8).

III. RESULTS

To test the accuracy of the melting criterion and reproducibility of the results of the described heating procedure, we flash heated a $30\text{-}\mu\text{m}$ -thick polished Ta foil in an argon gas flow at one atmosphere below and above the known melting temperature of 3270 K [37,38] (Fig. 3). The argon environment prevented any detectable chemical reaction upon heating for all temperatures, as checked in the EDX, in stark contrast to experiments in air. The EDX instrument used can detect 0.1–0.2% of oxygen (O) and carbon (C), and at 25 keV the incident electron beam probes a depth of about 800 nm. In a separate comparative study using EDX conducted at 5, 15, and 25 keV, with the instrument calibrated using a Ta standard specimen, the source of traces of O and C was found to be only on the surface and not in the bulk of the material.

At 3195 K, the first melt feature in the form of a crater is seen in the SEM image. At 3267 K, depth profiling using FIBM showed restructuring of material, several micrometers in depth and diameter, with a sharp boundary. We thus conclude that melting starts at 3195 K, but the amount of melt is too small to be visible in the depth profile compared to that for 3267 K. Given the age of the literature values for melting temperatures at 1 atm ranging from 3200 to 3300 K, we suggest a slight

downward correction based on our more accurate calibration procedures [39].

As a melt criterion at higher pressure, we thus use the first textural modification (onset of melting) as a lower bound of the melting temperature and the restructuring of the bulk material in depth as an upper bound. Typically, these bounds lie within 100 K for Ta.

Out of the total 71 runs carried out, we report 42 here. Discarded runs include test runs to optimize the laser power, laser defocusing, and flash-heating duration, along with a few experimental runs with unsatisfactory Planck fits, optical misalignment, or suspected chemical impurity. To check the possible chemical contamination or structural modifications during sample preparation using laser cutting, we carried out flash-heating test runs on samples prepared by FIBM and found no differences in the melting temperatures.

Figure 4 shows microscope pictures of Ta discs for two separate runs (A1 \rightarrow A4, B1 \rightarrow B4) before and after flash heating at 35 GPa, and after recovery to ambient pressure. At 35 GPa and 3709 K, there is no change after flash heating, whereas at 3845 K, a shiny crater is formed. Samples recovered to ambient conditions from the same pressure but quenched from temperatures differing by $\cong 135\ \text{K}$ show concave, rough features contrasting the convex, shiny, smooth melt features. These samples were further analyzed using SEM, FIBM, and EDX probes (Fig. 5). In contrast to the unchanged textural appearance to several micrometers in depth at 3709 K, the FIB cross section at 3845 K shows a clear boundary separating the unmolten and the restructured quenched molten portion. The EDX at 25 keV on these samples revealed no chemical reaction upon flash heating.

As another example of flash heating, Fig. 6 shows stages of two separate runs (two vertical panels) on two different

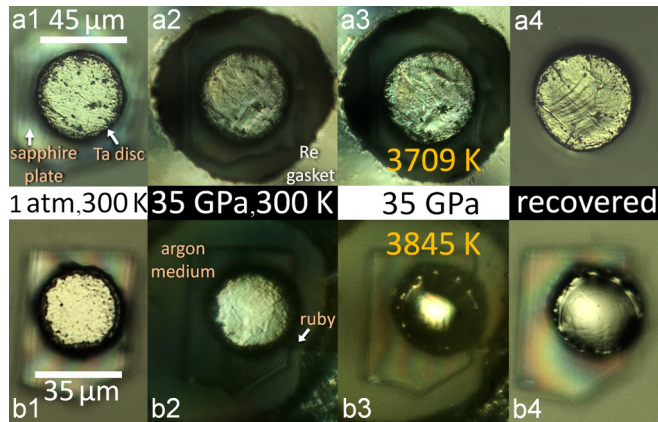


FIG. 4. Microphotographs of Ta discs at different stages of two separate flash-heating runs at 35 GPa. a1, b1: Ta discs placed on thin sapphire plates at 1 atm. a2, b2: Same discs loaded to 35 GPa in the DAC before heating. a3, b3: discs after flash heating to 3709 K and 3845 K, respectively. In b3, formation of a shiny, smooth circular crater was observed, in contrast to a3. a4, b4: Features retained on the discs recovered from the respective high P-T conditions. Scale bars shown are for the respective rows.

samples carried out at 50 GPa. The microphotographs of Ta discs before (A, B) and after flash heating (A', B') show that at 3906 K there is no change after flash heating, whereas at 3975 K, a shiny crater is formed. Likewise the 35 GPa run, the

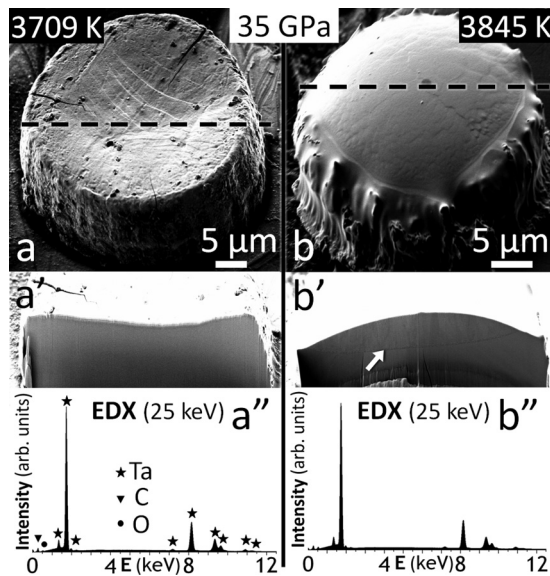


FIG. 5. Ta discs, recovered from two separate flash-heating runs at 35 GPa, as probed by SEM, FIBM, and EDX. a, b: SEM images of discs heated to 3709 K and 3845 K, respectively. The difference between the surface textures for these temperatures is significant, and the melt features are similar to the one atmosphere test. Respective FIB cross sections a', b' are cut through the hot spot areas. No change in textural appearance in the depth in a' contrasts a sharp boundary in b', extending a few micrometers in depth, separating quenched liquid and the unmolten solid. Respective EDX spectra in a'', b'' indicate no chemical alteration upon melting. Scale bars shown are for the respective vertical panels.

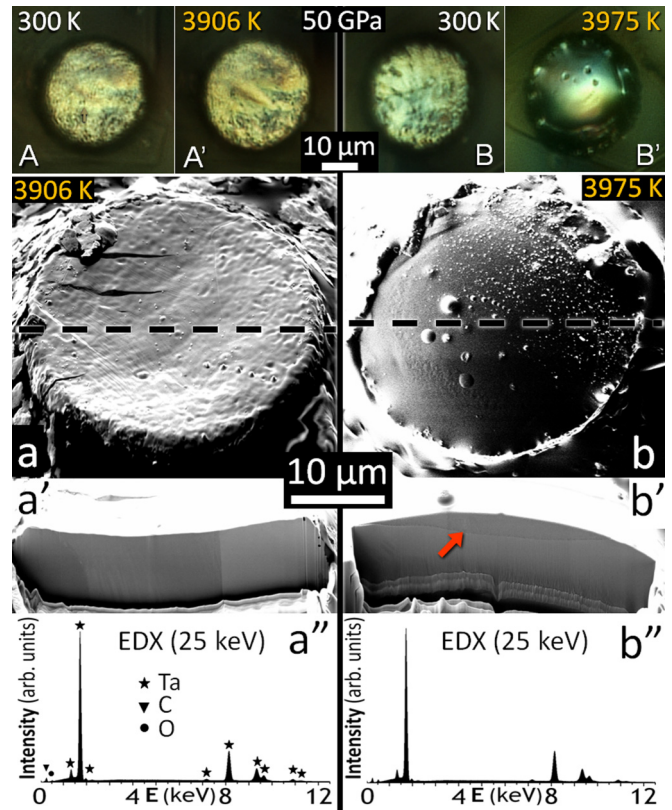


FIG. 6. Optical, SEM, FIBM, and EDX analysis of Ta discs in two separate flash-heating runs at 50 GPa. The two vertical panels pertain to two separate runs on two different samples. Row 1: Microphotographs of Ta discs placed on thin sapphire plates loaded to 50 GPa in argon in the DAC before heating (A, B) and after flash heating to 3906 K and 3975 K (A', B'), respectively. In B', formation of a shiny, smooth circular crater was observed, in contrast to A'. a, b: SEM images of the recovered discs. The difference between the surface textures is significant, and the melt features are similar to the 1 atm test (Fig. 3). a', b': SEM images of the respective FIB cross sections cut through the hot spot areas. Unaltered textural appearance in depth in a' contrasts a sharp boundary shown by a red arrow in b', extending to a few micrometers in depth, separating the quenched liquid and the unmolten solid. a'', b'': Respective EDX spectra indicate no chemical alteration upon melting.

convex, shiny, smooth melt features that contrast the concave, rough, solid features are retained upon recovery to ambient conditions. A further analysis using SEM and FIBM reveals that in contrast to the cross section at 3906 K (a'), the one at 3975 K (b') shows a clear boundary between the unmolten and the restructured quenched molten portion. The EDX on these samples confirmed an absence of chemical reactions. The described FIB profiles at 35 and 50 GPa, shown in Fig. 7 for clarity, reveal the extent of melt to several micrometers in depth.

The SEM and EDX were performed for all 42 runs, and FIBM was done whenever depth profiling was required. In Fig. 8, the P-T conditions leading to no textural modifications are assigned as solid, those showing melt features to several micrometers in depth are molten, and those with textural modification on the surface are onset, representing the lower bound of the melting curve as discussed earlier. We report the

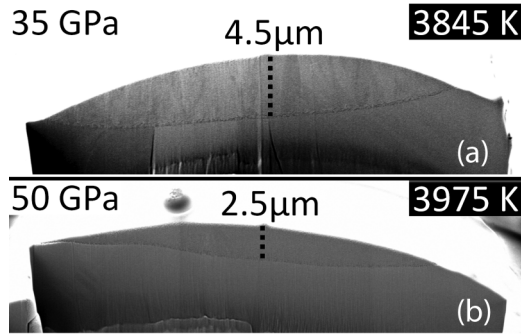


FIG. 7. FIB cross sections of Ta discs recovered from (a) 35 GPa, 3845 K and (b) 50 GPa, 3975 K showing the extent of the molten portions.

melting temperatures, shown in Fig. 1, corresponding to the onset with an uncertainty equal to the difference between the highest solid temperature and the lowest molten temperature. At 85 GPa, the melt features were observed only at 4318 K [Fig. 9(b)]. Due to insufficient number of runs at this pressure (Fig. 8), we conclude from the uncertainties in the lower pressure runs, that the melting curve must lie within ± 100 K of this temperature.

IV. DISCUSSION

The differences between the present and previous LHDAC results may be explained as follows: The previously used laser speckle method [1] attributes the onset of melting to laser-speckle motion due to textural changes of the sample

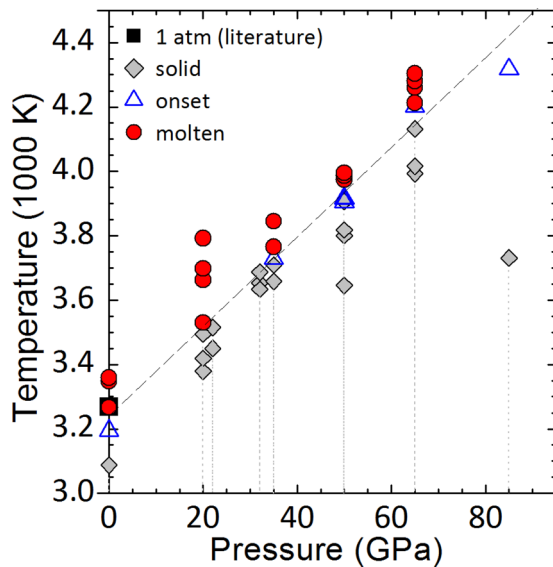


FIG. 8. Flash-heating data on Ta in the LHDAC. Each data point is the result of a single flash-heating event on a new Ta disc. Filled gray diamonds: solid - no textural modifications observed on the surface and in depth of material; open blue triangles: onset - the first melt features appeared; filled red circles: molten - restructuring of material observed with quenched liquid-solid boundary extending to several micrometers deep. At 85 GPa, only an onset and a solid data point were measured. The solid data point lies on the previous flat melting data [1,19]. The dashed line is a guide to the eye.

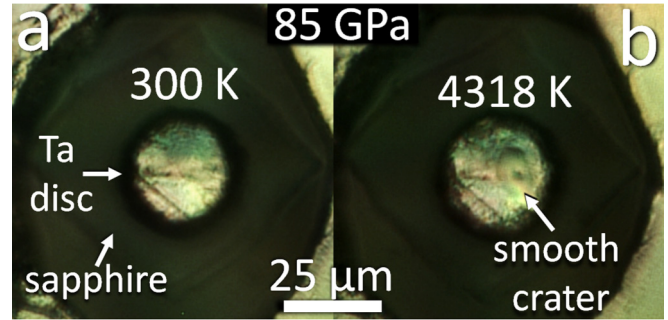


FIG. 9. Microphotographs of Ta at 85 GPa in the LHDAC. At 85 GPa, a Ta disc resting on a sapphire plate in argon in the DAC is shown before heating (a) and after flash heating to 4317 K (b). The smooth crater in b clearly indicates melting.

surface during melting. It has been reliably used for many materials from different classes. Yet, for Ta, it underestimated the melting temperature, e.g., by 500 K at 85 GPa (Fig. 1). Such a large discrepancy cannot be explained by experimental uncertainties and must therefore be due to chemical contamination caused by long heating durations [20]. The same applies for the earlier XRD measurements [19].

With regards to the large uncertainties in melting temperatures reported from the recent LHDAC-XRD experiments [20], we conclude that these must have been due to a combination of a misalignment while measuring temperatures due to sample instabilities as discussed earlier and the chemical reactions of the sample reported in that study itself. In the absence of sample instabilities and contaminations, the XRD measurements on their 5-μm-thick samples using double-sided heating should have been able to detect the substantial melt portion, as evident from our Fig. 7.

V. CONCLUSION

In contrast to the recent XRD measurements on melting of tantalum, which showed large uncertainties, the present melting curve cannot be reconciled with shock measurements and theoretical predictions. Flash heating combined with SEM, FIBM, and EDX analysis on the recovered samples produced significantly more accurate data to 85 GPa than previous melting experiments with melting temperatures bracketed within ± 100 K. The textural modifications are very reproducible and unambiguous, and chemical contaminations are carefully monitored for the first time to ensure sample purity. The present paper solves the two major problems in melting experiments: detection of the onset of melting and chemical contamination.

ACKNOWLEDGMENTS

This paper was supported as part of Energy Frontier Research in Extreme Environments Center (EFree), an Energy Frontier Research Center funded by the U.S. Department of Energy, Office of Science under Award No. DE-SC0001057 and was funded in part by the Carnegie-DOE Alliance Center, Grant No. DE-NA0002006. We thank Y. Meng, R. Hrubciak, T. Strobel, M. Guthrie, and B. Haberl for XRD measurements and C. Crispin and J. Armstrong for their help in FIBM and SEM.

- [1] D. Errandonea, B. Schwager, R. Ditz, C. Gessmann, R. Boehler, and M. Ross, *Phys. Rev. B* **63**, 132104 (2001).
- [2] J. A. Moriarty, *Phys. Rev. B* **49**, 12431 (1994).
- [3] Y. Wang, R. Ahuja, and B. Johansson, *Phys. Rev. B* **65**, 014104 (2001).
- [4] J. A. Moriarty, J. F. Belak, R. E. Rudd, P. Söderlind, F. H. Streitz, and L. H. Yang, *J. Phys.: Condens. Matter* **14**, 2825 (2002).
- [5] A. B. Belonoshko, S. I. Simak, A. E. Kochetov, B. Johansson, L. Burakovsky, and D. L. Preston, *Phys. Rev. Lett.* **92**, 195701 (2004).
- [6] A. Strachan, T. Çağın, O. Gülseren, S. Mukherjee, R. E. Cohen, and W. A. Goddard III, *Model. Simul. Mater. Sci. Eng.* **12**, S445 (2004).
- [7] A. K. Verma, R. S. Rao, and B. K. Godwal, *J. Phys.: Condens. Matter* **16**, 4799 (2004).
- [8] C. Cazorla, M. J. Gillan, S. Taioli, and D. Alfè, *J. Chem. Phys.* **126**, 1 (2007).
- [9] M. Foata-Prestavoine, G. Robert, M. H. Nadal, and S. Bernard, *Phys. Rev. B* **76**, 104104 (2007).
- [10] M. Ross, D. Errandonea, and R. Boehler, *Phys. Rev. B* **76**, 184118 (2007).
- [11] S. Taioli, C. Cazorla, M. J. Gillan, and D. Alfè, *Phys. Rev. B* **75**, 214103 (2007).
- [12] A. B. Belonoshko, L. Burakovsky, S. P. Chen, B. Johansson, A. S. Mikhaylushkin, D. L. Preston, S. I. Simak, and D. C. Swift, *Phys. Rev. Lett.* **100**, 135701 (2008).
- [13] Z. L. Liu, L. C. Cai, X. R. Chen, and F. Q. Jing, *Phys. Rev. B* **77**, 024103 (2008).
- [14] F. Xi and L. Cai, *Phys. B* **403**, 2065 (2008).
- [15] C. Wu, P. Söderlind, J. Glosli, and J. Klepeis, *Nat. Mater.* **8**, 223 (2009).
- [16] L. Burakovsky, S. P. Chen, D. L. Preston, A. B. Belonoshko, A. Rosengren, A. S. Mikhaylushkin, S. I. Simak, and J. A. Moriarty, *Phys. Rev. Lett.* **104**, 255702 (2010).
- [17] Z. Y. Zeng, C. E. Hu, X. Liu, L. C. Cai, and F. Q. Jing, *Appl. Phys. Lett.* **99**, 191906 (2011).
- [18] J. Ruiz-Fuertes, A. Karandikar, R. Boehler, and D. Errandonea, *Phys. Earth Planet. Inter.* **181**, 69 (2010).
- [19] D. Errandonea, M. Somayazulu, D. Häusermann, and H. K. Mao, *J. Phys.: Condens. Matter* **15**, 7635 (2003).
- [20] A. Dewaele, M. Mezouar, N. Guignot, and P. Loubeyre, *Phys. Rev. Lett.* **104**, 255701 (2010).
- [21] J. M. Brown and J. W. Shaner, in *Shock Waves Condensed Matter—1983*, edited by J. R. Asay, R. A. Graham, and G. K. Straub (Elsevier, Amsterdam, 1984), pp. 91–94.
- [22] C. Dai, J. Hu, and H. Tan, *J. Appl. Phys.* **106**, 043519 (2009).
- [23] J. Li, X. Zhou, J. Li, Q. Wu, L. Cai, and C. Dai, *Rev. Sci. Instrum.* **83**, 053902 (2012).
- [24] J. B. Haskins, J. A. Moriarty, and R. Q. Hood, *Phys. Rev. B* **86**, 224104 (2012).
- [25] L. M. Hsiung and D. H. Lassila, *Scr. Mater.* **39**, 603 (1998).
- [26] Y. Yao and D. D. Klug, *Phys. Rev. B* **88**, 054102 (2013).
- [27] Z. L. Liu, L. C. Cai, X. L. Zhang, and F. Xi, *J. Appl. Phys.* **114**, 073520 (2013).
- [28] J. Hu, C. Dai, Y. Yu, Z. Liu, Y. Tan, X. Zhou, H. Tan, L. Cai, and Q. Wu, *J. Appl. Phys.* **111**, 033511 (2012).
- [29] P. A. Rigg, R. J. Scharff, and R. S. Hixson, *J. Phys. Conf. Ser.* **500**, 032018 (2014).
- [30] P. Söderlind and J. A. Moriarty, *Phys. Rev. B* **57**, 10340 (1998).
- [31] H. Cynn and C. S. Yoo, *Phys. Rev. B* **59**, 8526 (1999).
- [32] A. Dewaele, M. Mezouar, N. Guignot, and P. Loubeyre, *Phys. Rev. B* **76**, 144106 (2007).
- [33] L. Yang, A. Karandikar, and R. Boehler, *Rev. Sci. Instrum.* **83**, 063905 (2012).
- [34] R. Boehler, *Rev. Sci. Instrum.* **77**, 115103 (2006).
- [35] Y. Akahama and H. Kawamura, *J. Appl. Phys.* **96**, 3748 (2004).
- [36] R. Boehler, M. Ross, P. Söderlind, and D. B. Boercker, *Phys. Rev. Lett.* **86**, 5731 (2001).
- [37] L. Malter and D. Langmuir, *Phys. Rev.* **55**, 743 (1939).
- [38] J. W. Shaner, G. R. Gathers, and C. Minichino, *High Temp. High Press.* **9**, 331 (1977).
- [39] R. Boehler, *Hyperfine Interact.* **128**, 307 (2000).
- [40] N. S. Fateeva and L. F. Vereshchagin, *Sov. Phys. DOCKLADY* **16**, 322 (1971).
- [41] R. Boehler, H. G. Musshoff, R. Ditz, G. Aquilanti, and A. Trapananti, *Rev. Sci. Instrum.* **80**, 045103 (2009).